European Journal of Inorganic Chemistry

EurJIC
European Journal of Inorganic Chemistry

Chemistry Europe
European Chemical Societies Publishing

RESEARCH ARTICLE

Balancing Structural Properties to Improve Quantum Yields in Zinc-Based Halometallate Films

Alison M. Costello[1] | Chloe Shamel[1] | James McDaniel[1] | Nipun Chandrasiri[1] | R. Nicholaus Quammen[2] | Sean A. Parkin[1] | Doo Young Kim[1] | Aron J. Huckaba[1]

[1]Department of Chemistry, University of Kentucky, Lexington, Kentucky, USA | [2]Center for Nanoscale Science and Engineering, University of Kentucky, Lexington, Kentucky, USA

Correspondence: Aron J. Huckaba (aron.huckaba@uky.edu)

Received: 19 May 2026 | **Revised:** 9 September 2026 | **Accepted:** 14 September 2026

Keywords: amorphous solid | conjugated system | halide | light emission | materials science | metal halides | steric effects | thin film | zinc

ABSTRACT

Lead halide perovskites are highly sought after for optoelectronic applications due to their tunable bandgaps and high quantum yields. However, concerns regarding lead toxicity and stability have driven research toward alternative materials, such as organic–inorganic metal halides or halometallates. Among these, low-dimensional, zero-dimensional structures show significant promise. Zinc has emerged as an abundant, low-cost, nontoxic candidate to replace lead, particularly for blue light emission. While previous studies focused on nonconjugated organic cations yielding "ultrastable" materials, this article investigates the impact of using light-absorbing, conjugated organic cations instead. The optical properties of 15 different conjugated materials were studied in both the solution phase and as thin films. By varying naphthalimide isomers with piperidinyl organic pendants having different cation steric bulk and anion size, the study examines emissive properties in spin-coated amorphous Zn-based OIMH films to show that photoluminescence efficiency in these materials can be improved, ultimately leading to films with PLQYs of up to 29% of an HCl salt of the organic cation and 26% for one of the hybrid materials.

1 | Introduction

Lead halide perovskites are promising materials that can be solution processed for many applications including light-emitting diodes, solar cells, and sensors [1–6]. LHPs are coveted for their tunable bandgaps, ability to tolerate defects, and high quantum yields [7–9]. Recently, a popular field of study into organic–inorganic metal halides (OIMHs), also called halometallate, has emerged. These structures are similar to LHPs but lack a few defining features. In LHPs, each of the halide ligands is shared between neighboring Pb octahedra, and the small monovalent cations are in the interstitial spaces between octahedra, generating a highly symmetrical structure. However, in OIMHs, the halides are shared to a much lesser degree, which greatly impacts material properties. Therefore, they should not be referred to as perovskites [10]. OIMHs can be two-dimensional (2-D), one-dimensional, or zero-dimensional (0-D), or mixtures of the above, termed quasi-structures. They have gained popularity due to their increased water stability in reference to LHPs and optoelectronics property tunability. 0-D halometallates specifically are discrete metal halide centers surrounded by organic cations [7, 10–12]. While LHPs are under intense study, due to the concern of lead toxicity in these materials, much effort is underway to find a stable lead-free alternative material [13, 14].

One metal identified as a potential candidate to replace lead, especially as a material for blue light emission, is zinc. Zinc is an abundant, low-cost, nontoxic metal [15]. Both Li et al. and Ma et al. have shown that zinc is a promising candidate to replace lead in low-dimensional halometallates [16, 17]. They have shown that bulk crystals and microscale powders can have high photoluminescent quantum yields. Ma et al. specifically reported that zinc-based halometallates are "ultra stable" in a

All rights reserved, including rights for text and data mining and training of artificial intelligence technologies or similar technologies.
© 2026 Wiley-VCH GmbH.

variety of conditions. The series of organic molecules in the 0-D materials they reported are molecules with little to no conjugation. Thus, it led us to the question: what if the organic cations themselves used were light-absorbing?

In this article, we investigate the optical properties of 15 different organic and hybrid materials containing an organic cation with an appended conjugated organic moiety in the solution phase and as thin films to determine how certain molecules aggregate to form "dark states" that are not emissive when they are in films. The hybrid materials are novel, as are the organic molecules they are derived from. We pair different orientations of naphthalimide core, different cation steric bulk, and different anion sizes, resulting in a range of emission properties. We found after spin coating that films of amorphous Zn-based OIMHs had PLQYs of 26% and 29%.

2 | Results and Discussion

2.1 | Synthesis of Organic Cations

The synthesis of the organic cation precursors began with a condensation reaction between an aminopiperidine and a naphthalic anhydride (Figure 1). Nuclear magnetic resonance spectra are provided in the Supporting Information (Figures S1–S10). We varied the specific position of the anhydride moiety to vary the type and amount of π–π interaction possible between cations in the OIHM material. In this series, 1,8-naphthalic anhydride, 1,2-naphthalic anhydride, and 2,3-naphthalic anhydride are used. For the first series, 4-amino-2,2,6,6-tetramethyl piperidine (TMP) was condensed with a series of isomeric naphthalic anhydrides. In the second series, piperidine (P) required a Boc-protected 4-(aminomethyl) piperidine as the unprotected piperidine nitrogen caused deleterious side reactions to occur. The desired piperidine-substituted molecule was therefore obtained after a deprotection step, which also yielded the desired ammonium chloride salt. For the TMP series of molecules, the compounds were dissolved in dichloromethane (DCM), and an excess of concentrated HCl was added. The reaction was stirred for an hour, and then the mixture was dried under reduced pressure. The 1,2-P cation was not synthesized due to deleterious side reactions. Many reaction conditions were tried, but each time the Boc protecting group was replaced by a formyl group that was reasoned to come from the DMF solvent. Each attempt at synthesizing 1,2-P resulted in very poor yields of the formyl product, that was subsequently unable to be deprotected.

2.2 | Synthesis of Halometallate Materials

After the organic cations were synthesized, halometallate materials were formed. This was accomplished by dissolving a cation and zinc chloride in a 2:1 molar ratio in minimal ethanol and adding 5 molar equivalents of HCl. The reaction was stirred for 30 min, and then the product was dried under vacuum.

2.3 | Photophysical Properties

The UV–vis absorbance and steady-state emission spectra of the neutral organics, the HCl salts, and the halometallates are shown in Figures 2 and 3, respectively. Further UV–vis absorbance spectra (Figures S11–S16) and photoluminescence spectra (Figures S17–S21) are provided in the Supporting Information. The films were determined to be amorphous glasses in nature, as revealed by powder X-ray diffraction data (Figures S31–S45). This indicated that the films had no long-range order. Compared to the solution phase UV–vis spectra, the solid phase UV–vis spectra show a varying degree of redshifted absorption signal for each material. This indicated the presence of J aggregates in the solid state. There is also a loss of fine structure in the thin-film spectra to various degrees, as evidenced by the differing breadth of signals in comparison to their solution counterparts. The observed changes are not expected to be due to the presence of the piperidine groups as they are not conjugated. There is also no change in spectra between the unprotonated organic compound, the cation, and the halometallate in solution. The

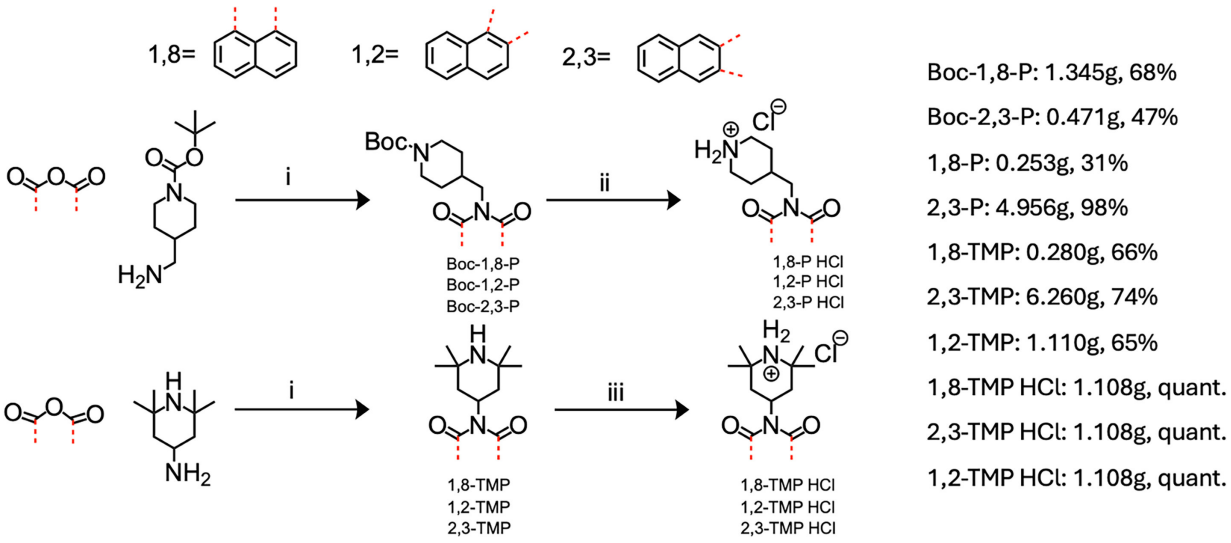

FIGURE 1 | Synthetic scheme of organic cations for halometallate formation. Reaction conditions: (i) cat. imidazole, DMF, reflux. (ii) 4 M HCl in DCM, rt. (iii) EtOH, excess HCl, rt.

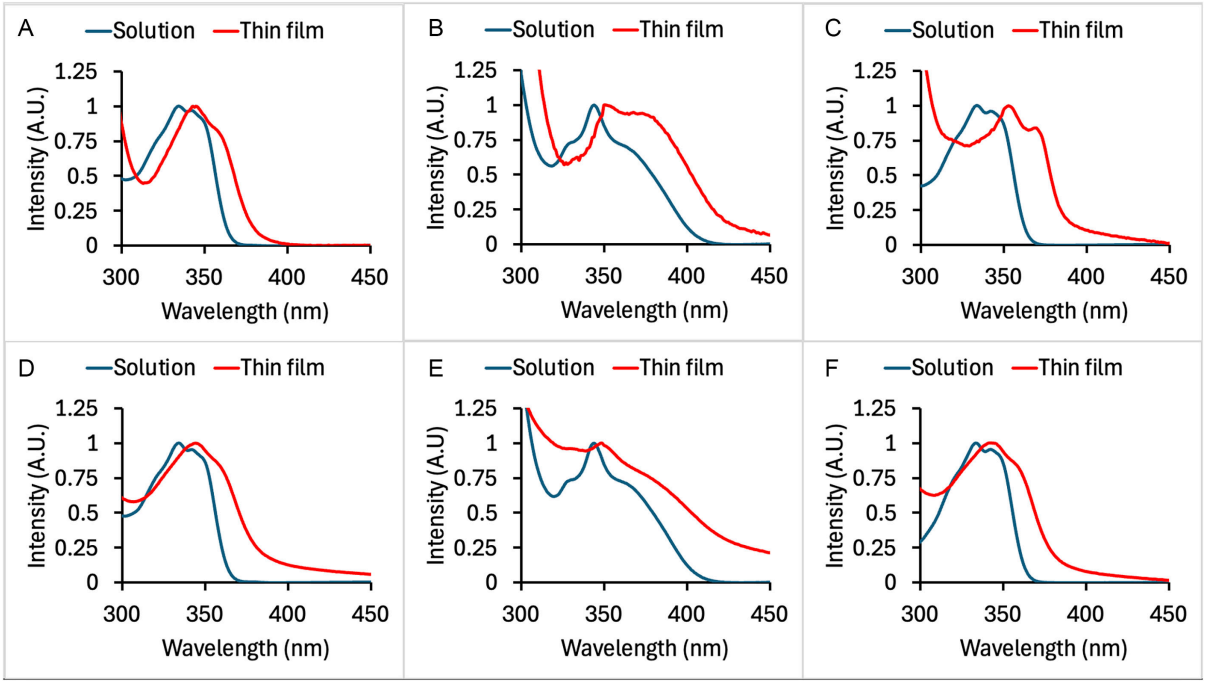

FIGURE 2 | (A) Normalized UV–vis spectra of 1,8-TMP HCl in solution and thin film. (B) Normalized UV–vis spectra of 1,2-TMP HCl in solution and thin film. (C) Normalized UV–vis spectra of 1,8-P HCl in solution and thin film. (D) Normalized UV–vis spectra of $(1,8\text{-TMP})_2ZnCl_4$ in solution and thin film. (E) Normalized UV–vis spectra of $(1,2\text{-TMP})_2ZnCl_4$ in solution and thin film. (F) Normalized UV–vis spectra of $(1,8\text{-P})_2ZnCl_4$ in solution and thin film. Each solution phase spectrum was measured in ethanol.

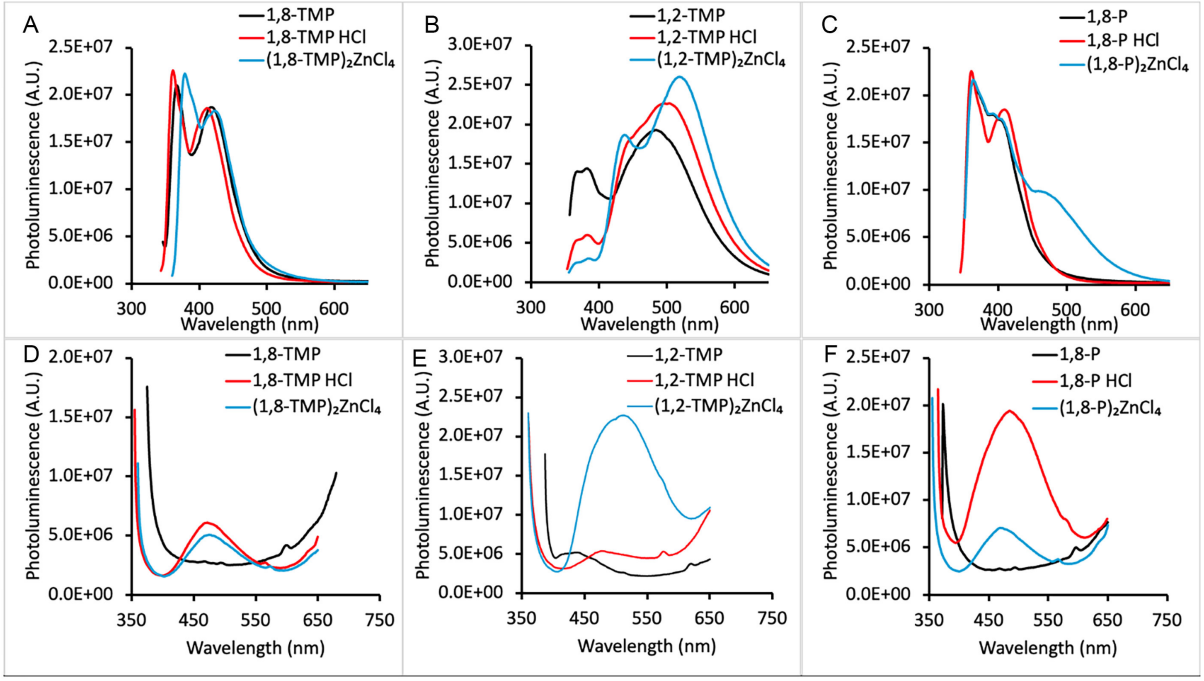

FIGURE 3 | Steady state emission spectra of: (A) 1,8-TMP series in ethanol. Solutions were excited at 345, 333, and 333 nm, respectively. (B) 1,2-Series in ethanol. Solutions were excited at 347, 343, and 346 nm, respectively. (C) 1,8-P series in ethanol. Solutions were excited at 346, 335, and 341 nm, respectively. (D) 1,8-TMP series thin films. Films were excited at 343, 345, and 350 nm, respectively. (E) 1,2-TMP series thin films. Films were excited at 377, 350, and 350 nm, respectively. (F) 1,8-P series thin films. Films were excited at 362, 354, and 345 nm, respectively.

light absorption characteristics of the materials in solution were deemed to be determined solely by the identity of the regioisomeric naphthalene moiety in the compound. This is to be expected as zinc chloride and piperidine derivatives do not absorb light in the same region [18, 19].

The $E_{0\text{–}0}$ values obtained by measuring where the UV–vis absorption and steady-state emission spectra (Figure 3) overlap indicated a low degree of Stokes shifting in the spectra, which we interpreted to mean little energy was lost to reorganization and excited-state structural relaxation.

The emission spectra of the thin films show that the neutral organic compounds alone show no emission. With the 1,8-TMP HCl and 1,8-P HCl salts, emission was observed, and the emission intensity was much greater for 1,8-P HCl. None of the 2,3-TMP samples exhibited emission. The 2,3-P series was similar, though no spectrum for 2,3-P HCl could be recorded due to difficulty in spin-coating a high-quality thin film. As for the zincate species, $(1,8\text{-TMP})_2ZnCl_4$ and $(1,8\text{-P})_2ZnCl_4$ show moderately intense emission, while $(1,2\text{-TMP})_2ZnCl_4$ shows much higher emission intensity, especially compared to the rest of the 1,2-TMP series. Because all the compounds were observed to be emissive in solution but not as thin films, we reasoned that aggregation of the compounds led to an increase in the nonradiative decay constant, likely due to aggregation. However, the thickness of the films must be considered (Table S2). After spin-coating and analysis by X-ray diffraction, the thickness of the films was analyzed by ellipsometry. Measurements were taken in three locations across the film and averaged. Each of the films was fabricated with inks of the same concentration and with the same spin-coating parameters. Even so, the resulting films were observed to have variable thickness. The neutral 1,8-P and 2,3-P exhibited ~100 nm thickness, but in general, the others were between ~30 and 60 nm. Looking first at the 1,8-TMP series, the HCl film is nearly half as thin as that of the zincate, 30 nm versus 52 nm, respectively. This change in thickness makes it hard to directly compare the magnitude of their absorbance and their fluorescence. For the 1,2-TMP series, the zincate has such a strong emission compared to the other two species in the series. 1,8-P series also had considerably different thicknesses. Because of the large differences in thickness we observed, we found conclusions difficult to draw. Based on this limited utility, we have made some observations. The 1,8-P film is much thicker than its counterparts, which may have contributed to the quenching of its fluorescence. The compounds in solution all have a similar emission profile. From this, it can be concluded that the nature of the emission results from the π* to π relaxation of the organic component of the materials. Furthermore, the lifetimes being in the tens of nanoseconds range indicates that there is likely no intersystem crossing, which also indicates simple prompt fluorescence after excitation.

Excited state lifetimes and quantum yields were recorded for the six compounds with appreciable emission (Figures S22–S30 and Table S1). Each of the observable lifetimes was on the scale of tens of nanoseconds (Table 1). Compared to recently reported $ZnBr_4$ OIMH materials, the lifetimes of these $ZnCl_4$ materials are ~10–20× shorter [17]. For materials containing a TMP moiety, the excited-state lifetimes were extended compared to the others when paired with the tetrachlorozincate anion. 1,8-TMP HCl had a lifetime of 6.41 ns compared to 13.44 ns for $(1,8\text{-TMP})_2ZnCl_4$—an approximately twofold increase in lifetime. Similarly, 1,2-TMP HCl had a lifetime of 6.52 ns, and $(1,2\text{-TMP})_2ZnCl_4$ had an approximately 2.5-fold increase, with the lifetime of 16.80 ns. For the 1,8-P substitution pattern, the HCl salt had an excited-state lifetime of 8.86 ns that was 2 times longer than that of the tetrachlorozincate (4.68 ns).

The quantum yields of the thin films of the materials followed the same trend as the lifetimes; however, a quantum yield could not be determined for 1,2-TMP and 1,8-TMP as the emission intensity was too low. $(1,2\text{-TMP})_2ZnCl_4$ and 1,8-P HCl had the highest PLQY values at 26.5% and 28.8%, respectively. The quantum yields for the other materials were below 7%. The quantum yields of $(1,2\text{-TMP})_2ZnCl_4$ and 1,8-P HCl are slightly lower but comparable to the state-of-the-art for $ZnBr_4$ halometallates, which range from 35.5% to 20.3% [17]. They are also similar to values for selected lead-based 2-D and 0-D halometallates, which have reported efficiencies of 28.8% and 26% [20, 21]. Based on the lifetime and quantum yield data we've collected, we reasoned that the steric bulk both the TMP cation and of the $ZnCl_4$ dianion may reduce the amount of intermolecular interaction between the emissive naphthalene diimide molecules (Table 1, Figure 4, vide infra). The same trend of increasing lifetime and quantum yield was observed in the 1,8- and 1,2-isomer series (Table 1).

2.4 | Crystallography

During the course of these studies, we sought to investigate the structure of each material in an effort to compare any intermolecular interactions that may be present. We rationalized that even though the films we cast and studied above were not highly crystalline, understanding basic patterns of how the ions interact in the solid

TABLE 1 | Table summarizing photophysical properties of a select number of tested compounds.

Compound	ε, L mol^{-1} cm^{-1}	λ_{max}, nm (solution, thin film)	$E_{0\text{-}0}$, eV (solution, thin film)	Emission max, nm (solution, thin film)	Thin film PLQY, %	Thin film lifetime, ns
1,8-TMP	10 344	335, 347	3.48, —[a]	367, —[a]	—[a]	—[a]
1,8-TMP HCl	13 844	335, 343	3.49, 3.08	361, 472	3%	6.41
$(1,8\text{-TMP})_2ZnCl_4$	26 772	334, 344	3.41, 2.97	379, 475	7%	13.44
1,2-TMP	2168	344, 376	3.43, —[a]	484, —[a]	—[a]	5.40
1,2-TMP HCl	3230	344, 351	3.09, 2.87	558, 479	7%	6.52
$(1,2\text{-TMP})_2ZnCl_4$	4965	344, 348	3.10. 2.86	563, 511	26%	16.80
1,8-P	9919	334, 361	3.49, —[a]	364, —[a]	—[a]	—[a]
1,8-P HCl	11 874	334, 353	3.50, 3.02	361, 484	29%	8.86
$(1,8\text{-P})_2ZnCl_4$	25 034	334,343	3.50, 3.00	364, 470	0%[b]	4.68

[a]Compound had no thin film emission and therefore these values could not be calculated.
[b]Calculated PLYQ was rounded to zero.

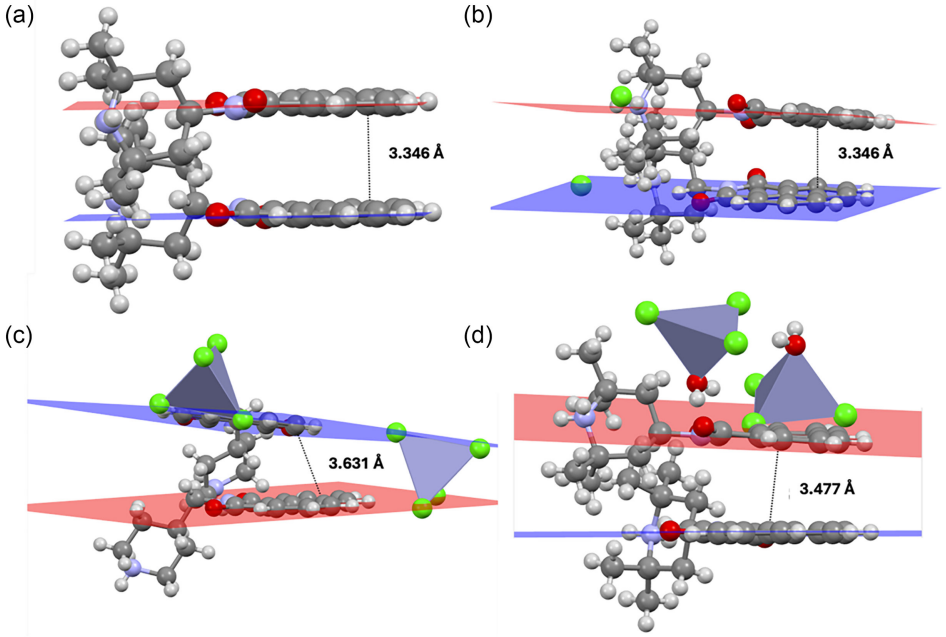

FIGURE 4 | Crystal structures and representative molecular distances of (a) 1,8-TMP with solvating CH_2Cl_2 removed, (b) 1,8-TMP HCl, (c) $(1,8\text{-P})_2ZnCl_4$ and (d) $(1,8\text{-TMP})_2ZnCl_4$. 1,8-Naphthalenediimide planes highlighted in red and blue to illustrate the parallel nature of the two rings in each pair.

state in general could be useful. Crystals suitable for X-ray crystallography were grown for several of the compounds, their cations, and the halometallates (Figures 4 and 5, Tables S3–S6). The complete 1,8-TMP series was crystallized and is shown in Figure 4, along with $(1,8\text{-P})_2ZnCl_4$.

From the crystal structures in Figure 4, the overlap in the conjugated portion of the organic cations is evident, as is the relative tilt of one ring in reference to the other in each pair, which suggests some degree of intermolecular interactions between the aromatic moieties. N each material, a slip-stack packing arrangement was observed, with the biggest difference being the distance between the polyaromatic ring's centroid (3.89 Å for 1,8-TP, 4.33 Å for 1,8-TMP HCl, 4.277 Å for $(1,8\text{-P})_2ZnCl_4$, and 3.477 Å for $(1,8\text{-TMP})_2ZnCl_4$). While physical overlap does not entirely predict electronic coupling when they are well separated, as seen in the $(1,8\text{-TMP})_2ZnCl_4$ crystal

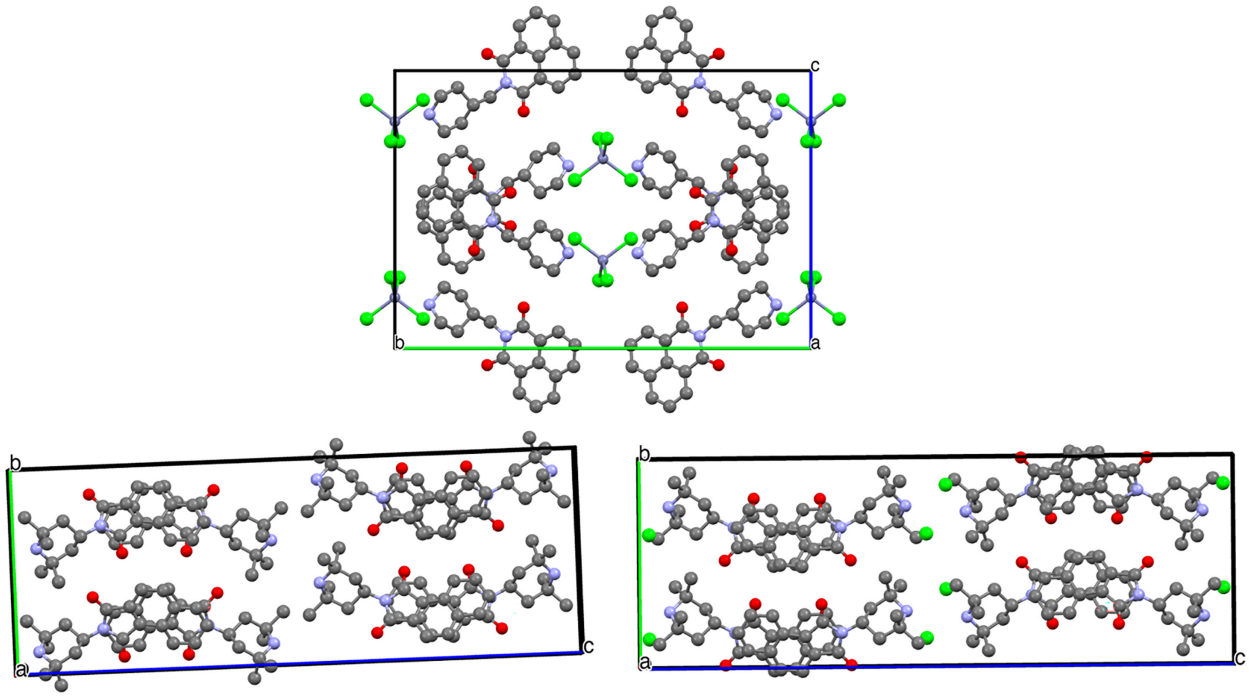

FIGURE 5 | Crystal structures of $(1,8\text{-P})_2ZnCl_4$ with solvating water removed (top center), 1,2-TMP (bottom left), and 1,2-TMP HCl (bottom right). Hydrogens omitted for clarity.

structure, it is likely there is some electronic coupling. This means that in the crystalline state, the excited-state electron and hole are less likely to recombine to emit light [22]. Even so, the low crystallinity of the films (*vide supra*) precludes our ability to make wide connections between film and single crystal.

2.5 | Comparative Structure–Property Discussion

In the TMP series, which was the most sterically large ammonium organic pendant used here, each of the neutral organic isomers studied was not emissive in the solid state. Upon protonation to the HCl salt, however, each (with the exception of the *2*,*3*-isomer) was found to be emissive, even if weakly so. Increasing the steric bulk of the anion from chloride to tetrachlorozincate translated to an increase in the PLQY for the TMP series of materials, while for the P series, the chloride exhibited the highest emission quantum efficiency. Furthermore, increasing the size of the anion steric bulk (from no anion to chloride to tetrachlorozincate) also increased the wavelength of the observed emission in the solution phase and increased the excited-state lifetime with the same basic trends as the PLQY. Additionally, the molar absorptivity of the dissolved halometallate increased with the same trend. In both the TMP and P series, absorptivity increased with protonation and then also with conversion of Cl to $ZnCl_4$.

3 | Conclusion

Zinc-based halometallate materials are attractive materials for light emission applications due to zinc being inexpensive and more environmentally friendly than lead-based materials. Here, we have synthesized a series of 15 materials to investigate how the optoelectronic properties differ when comparing molecules with different steric hinderance, anions of different sizes, and isomeric naphthalene. The materials were investigated in both the solution phase and as amorphous films. Trends in emission intensity, lifetimes, and quantum yields show that the sterically hindered TMP linker provides higher intensity and photoluminescence quantum yields with the larger $ZnCl_4$ anion. Alternatively, the less sterically demanding cation (P series) showed stronger emission, longer lifetimes, and higher quantum yields with the smaller chloride anion. This indicates that there likely is some balance to be struck to promote beneficial interactions while limiting deleterious interactions. However, difference in film thicknesses may also play a role in the quenching or intensity of the emission. The steric hinderance of the piperidine linker and the size of the anion likely influence proximity between organic moieties. If the molecules are not properly spaced, aggregation could lead to dark processes, which are deleterious for light emission. The materials with highest PLQY were $(1,2\text{-TMP})_2ZnCl_4$ (26.46%) and 1,8-P HCl (28.77%). For future studies, it would be beneficial to choose materials that readily form crystals and crystalline thin films for better comparisons between materials. Further, reducing any π–π overlap with more sterics may also increase lifetimes and PLQYs.

Acknowledgments

We thank the Eppley Foundation for funding this project.

Funding

This study was supported by Eppley Foundation for Research.

Conflicts of Interest

The authors declare no conflicts of interest.

Data Availability Statement

The data that support the findings of this study are available from the corresponding author upon reasonable request.

References

1. D. Li and J. Yu, "AIEgens-Functionalized Inorganic–Organic Hybrid Materials: Fabrications and Applications," *Small* 12, no. 47 (2016): 6478–6494, https://doi.org/10.1002/smll.201601484.

2. L. N. Quan, B. P. Rand, R. H. Friend, S. G. Mhaisalkar, T. W. Lee, and E. H. Sargent, "Perovskites for Next-Generation Optical Sources," *Chemical Reviews* 119, no.12 (2019): 7444–7477, https://doi.org/10.1021/acs.chemrev.9b00107.

3. K. Wang, D. Yang, C. Wu, M. Sanghadasa, and S. Priya, "Recent Progress in Fundamental Understanding of Halide Perovskite Semiconductors," *Progress in Materials Science* 106 (2019), https://doi.org/10.1016/j.pmatsci.2019.100580.

4. N. Zhang, K. Xia, Q. He, and J. Pan, "Recent Progress in the Stability of Red-Emissive Perovskite Nanocrystals for Light-Emitting Diodes," *ACS Materials Letters* 4, no. 6 (2022): 1233–1254, https://doi.org/10.1021/acsmaterialslett.2c00302.

5. A. Kojima, K. Teshima, Y. Shirai, and T. Miyasaka, "Organometal Halide Perovskites as Visible-Light Sensitizers for Photovoltaic Cells," *Journal of the American Chemical Society* 131, no. 17 (2009): 6050–6051, https://doi.org/10.1021/ja809598r.

6. Z. K. Tan, R. S. Moghaddam, M. L. Lai, et al., "Bright Light-Emitting Diodes Based on Organometal Halide Perovskite," *Nature Nanotechnology* 9, no. 9 (2014): 687–692, https://doi.org/10.1038/nnano.2014.149.

7. J. Almutlaq, J. Yin, O. F. Mohammed, and O. M. Bakr, "The Benefit and Challenges of Zero-Dimensional Perovskites," *Journal of Physical Chemistry Letters* 9 no. 14 (2018): 4131–4138, https://doi.org/10.1021/acs.jpclett.8b00532.

8. A. Chemmangat, J. Chakkamalayath, J. T. DuBose, and P. V. Kamat, "Tuning Energy Transfer Pathways in Halide Perovskite-Dye Hybrids Through Bandgap Engineering," *Journal of the American Chemical Society* 146, no. 5 (2024): 3352–3362, https://doi.org/10.1021/jacs.3c12630.

9. S. Nussbaum, E. Socie, L. Yao, J.-H. Yum, J.-E. Moser, and K. Sivula, "Tuning Napththalenediimide Cations for Incorporation Into Ruddlesden–Popper-Type Hybrid Perovskites," *Chemistry of Materials* 34, no. 8 (2022): 3798–3805, https://doi.org/10.1021/acs.chemmater.2c00246.

10. Q. A. Akkerman and L. What Manna, "What Defines a Halide Perovskite?" *ACS Energy Letters* 5, no. 2 (2020): 604–610, https://doi.org/10.1021/acsenergylett.0c00039.

11. L. Lian, M. Zheng, W. Zhang, et al., "Efficient and Reabsorption-Free Radioluminescence in Cs(3)Cu(2)I(5) Nanocrystals With Self-Trapped Excitons," *Advanced Science* 7, no. 11 (2020): 2000195, https://doi.org/10.1002/advs.202000195.

12. Y. Wu, N. Lv, X. Wang, et al., "UV-Curing Resin-Assisted Facile Synthesis of Lead-Free Zero-Dimensional Organic–Inorganic Hybrid Metal Halide Quantum Dots for Light-Emitting Application," *ACS Applied Nano Materials* 7, no. 19 (2024): 22802–22810, https://doi.org/10.1021/acsanm.4c03965.

13. A. Babayigit, D. Duy Thanh, A. Ethirajan, et al., "Assessing the Toxicity of Pb- and Sn-Based Perovskite Solar Cells in Model Organism Danio Rerio," *Science Reports* 6 (2016): 18721, https://doi.org/10.1038/srep18721.

14. A. Kumar and M. N. V. Prasad, "Plant-Lead Interactions: Transport, Toxicity, Tolerance, and Detoxification Mechanisms," *Ecotoxicology and Environmental Safety* 166 (2018): 401–418, https://doi.org/10.1016/j.ecoenv.2018.09.113.

15. B. Venditti, "Zinc Is Critical for the Low-Carbon Economy. Here's why," accessed March 17, 2025, https://www.weforum.org/stories/2022/04/zinc-low-carbon-economy-construction/2022.

16. D.-Y. Li, Y.-H. Liu, Q. Wang, X.-W. Lei, C.-Y. Yue, and Z.-H. Jing, "Zero-Dimensional Hybrid Zinc Halides With Blue Light Emissions," *Materials Today Chemistry* 31 (2023): 101604.

17. Y. Y. Ma, Y. M. Sun, W. J. Xu, et al., "Ultrastable 0D Organic Zinc Halides With Highly Efficient Blue Light Emissions," *Advanced Optical Materials* 10, no. 17 (2022), https://doi.org/10.1002/adom.202200386.

18. M. K. Trivedi, K. K. Sethi, P. Panda, and S. Jana, "A Comprehensive Physicochemical, Thermal, and Spectroscopic Characterization of Zinc (II) Chloride Using X-ray Diffraction, Particle Size Distribution, Differential Scanning Calorimetry, Thermogravimetric Analysis/Differential Thermogravimetric Analysis, Ultraviolet-Visible, and Fourier Transform-Infrared Spectroscopy," *International Journal of Pharmaceutical Investigation* 7, no. 1, (2017): 33–40, https://doi.org/10.4103/jphi.JPHI_2_17.

19. L. W. Pickett, M. E. Corning, G. M. Wieder, D. A. Semenow, and J. M. Buckley, "The Vacuum Ultraviolet Spectra of Cyclic Compounds. III. Amines," *Journal of the American Chemical Society* 75, no. 7 (1952): 1618–1622.

20. L. Dou, A. B. Wong, Y. Yu, et al., "Atomically Thin Two-Dimensional Organic–Inorganic Hybrid Perovskites," *Science* 349, no. 6255 (2015): 1518–1521, https://www.science.org/doi/abs/10.1126/science.aac7660.

21. L. J. Xu, A. Plaviak, X. Lin, et al., "Metal Halide Regulated Photophysical Tuning of Zero-Dimensional Organic Metal Halide Hybrids: From Efficient Phosphorescence to Ultralong Afterglow," *Angewante Chemie, International Edition* 59, no. 51 (2020): 23067–23071, https://doi.org/10.1002/anie.202010555.

22. Y. Gao, E. Shi, S. Deng, et al., "Molecular Engineering of Organic–Inorganic Hybrid Perovskites Quantum Wells," *Nature Chemistry* 11, no. 12 (2019): 1151–1157, https://doi.org/10.1038/s41557-019-0354-2.

Supporting Information

Additional supporting information can be found online in the Supporting Information section.